Split-Dose Technique for FDG PET/CT–guided Percutaneous Ablation: A Method to Facilitate Lesion Targeting and to Provide Immediate Assessment of Treatment Effectiveness[1]

E. Ronan Ryan, FFRRCSI
Constantinos T. Sofocleous, MD
Heiko Schöder, MD
Jorge A. Carrasquillo, MD
Sadek Nehmeh, PhD
Steven M. Larson, MD
Raymond Thornton, MD
Robert H. Siegelbaum, MD
Joseph P. Erinjeri, MD, PhD
Stephen B. Solomon, MD

Purpose: To describe a split-dose technique for fluorine 18 fluorodeoxyglucose (FDG) positron emission tomography (PET)/computed tomography (CT)-guided ablation that permits both target localization and evaluation of treatment effectiveness.

Materials and Methods: Institutional review board approved the study with a waiver of consent. From July to December 2011, 23 patients (13 women, 10 men; mean age, 59 years; range, 35–87 years) with 29 FDG-avid tumors (median size, 1.4 cm; range, 0.6–4.4 cm) were targeted for ablation. The location of the lesion was the liver (n = 23), lung (n = 4), adrenal gland (n = 1), and thigh (n = 1). Radiofrequency ablation was performed in 17 lesions; microwave ablation, in six; irreversible electroporation, in five; and cryoablation, in one. The pathologic condition of the tumor was metastatic colorectal adenocarcinoma in 18 lesions, primary hepatocellular carcinoma in one lesion, and a variety of metastatic tumors in the remaining 10 lesions. A total of 4 mCi (148 MBq) of FDG was administered before the procedure for localization and imaging guidance. At completion of the ablation, an additional 8 mCi (296 MBq) of FDG was administered to assess ablation adequacy. Results of subsequent imaging follow-up were used to determine if postablation imaging after the second dose of FDG reliably helped predict complete tumor ablation. Descriptive statistics were used to summarize the results.

Results: Twenty-eight of 29 (97%) ablated lesions showed no residual FDG activity after the second intraprocedural FDG dose. One patient with residual activity underwent immediate biopsy that revealed residual viable tumor and was immediately re-treated. Follow-up imaging at a median of 155 days (range, 92–257 days) after ablation showed local recurrences in two (7%) lesions that were originally negative at postablation PET.

Conclusion: Split-dose FDG PET/CT may be a useful tool to provide both guidance and endpoint evaluation, allowing an opportunity for repeat intervention if necessary. Further work is necessary to validate these concepts.

[1] From the Department of Radiology, Division of Interventional Radiology, Memorial Sloan-Kettering Cancer Center, 1275 York Ave, Suite H118, New York, NY 10065. Received July 28, 2012; revision requested October 1; revision received December 5; accepted December 20; final version accepted January 10, 2013. **Address correspondence to** S.B.S. (e-mail: *solomons@mskcc.org*).

Percutaneous tumor ablation requires intraprocedural imaging both to guide electrode placement and to determine the technical effectiveness and endpoint of the procedure (1). Placement of the ablation electrode is typically performed with ultrasonographic (US), computed tomographic (CT), or magnetic resonance (MR) imaging guidance. However, when the ablation target has the same echogenicity, attenuation, or signal intensity as the tissue that surrounds it, the lesion may be better visualized on fluorine 18 fluorodeoxyglucose (FDG) positron emission tomographic (PET) images. In these cases, investigators have fused, or registered, previously acquired PET scans with CT images obtained during the procedure (2). This approach is limited by challenges in accurate image registration, especially because procedural images are often obtained with the patient in positions and respiratory phases that differ substantially from prior diagnostic PET examinations.

Treatment effectiveness after tumor ablation can be assessed by using immediate imaging. Such assessments may prompt re-intervention if the intended ablation margin has not been achieved. Contrast material–enhanced CT, US, and MR imaging have all been used to assess and confirm ablation of the tumor and margin (3–8). However, while contrast-enhanced imaging techniques can depict the morphologic and perfusion changes caused by ablation, these techniques lack the metabolic information provided with PET imaging. FDG PET has been demonstrated to be a useful tool to assess the effectiveness of ablation by detecting the presence of residual or recurrent viable tumor tissue at follow-up at various time periods after the ablation, although inflammation can confound evaluation at early time points (9–12). Previous attempts with use of FDG PET at the time of the ablation to assess treatment adequacy failed to be helpful because FDG administered before the ablation remained localized within the treated tumors after ablation (13,14).

The objective of our study was to describe a technique for PET/CT-guided ablation that permits both target localization and evaluation of treatment effectiveness. We report our experience using a split-dose method of FDG PET/CT for ablation, whereby the standard administered diagnostic FDG activity dose of approximately 12 mCi (444 MBq) is administered in two aliquots: a 4-mCi (148-MBq) target dose administered before ablation and an 8-mCi (296-MBq) treatment efficacy dose administered immediately after the procedure.

Advance in Knowledge

- By using a split-dose method of fluorine 18 fluorodeoxyglucose (FDG) PET/CT imaging during tumor ablation we were able to successfully target the lesion and assess FDG activity at the end of the procedure, thus obtaining an immediate assessment of the completeness of ablation.

Implication for Patient Care

- The split-dose FDG PET protocol may offer a method of immediate assessment of completeness of a tumor ablation procedure.

Materials and Methods

Patients

From July to December 2011, 23 consecutive patients who had undergone split-dose FDG PET/CT-guided ablations for the treatment of 29 lesions were retrospectively identified from an institutional review board–approved, Health Insurance Portability and Accountability Act–compliant prospective database. All patients provided informed consent prior to PET/CT-guided ablations. Demographic information was collected for each patient from the medical record. Patients and lesion characteristics are summarized in Table 1.

Imaging and Ablation Protocol

Each PET/CT-guided intervention was performed according to a split-dose protocol as follows: The standard dose of 12 mCi (444 MBq) was divided into a targeting dose of 4 mCi (148 MBq) and a treatment efficacy dose of 8 mCi (296 MBq). The targeting dose of 4 mCi (148 MBq) was chosen on the basis of the FDG half-life and on our previous experience with the length of time a procedure takes before postablation imaging is performed such that approximately 10% of the dose is left at the end of the procedure. This consideration is meant to minimize the contamination from the preprocedure PET scan with the postprocedure scan.

Serum glucose levels were measured prior to the procedure. Patients were injected with approximately 4 mCi (148 MBq) of FDG about 1 hour prior to the procedure and were allowed to rest for about 1 hour prior to the procedure. Whenever possible, patients voided prior to transfer to the interventional PET/CT table. Imaging was performed with a GE Discovery 690 time-of-flight scanner (GE Healthcare, Waukesha, Wis). For all cases, general anesthesia with intubation and paralysis for full muscle relaxation was used. The patient was anesthetized on the PET/CT scanner prior to image acquisition. Then a 2-minute breath-hold PET acquisition of the organ to be targeted was performed at one table

Published online before print
10.1148/radiol.13121462 **Content code:** IR

Radiology 2013; 268:288–295

Abbreviation:
FDG = fluorine 18 fluorodeoxyglucose

Author contributions:
Guarantors of integrity of entire study, E.R.R., S.B.S.; study concepts/study design or data acquisition or data analysis/interpretation, all authors; manuscript drafting or manuscript revision for important intellectual content, all authors; approval of final version of submitted manuscript, all authors; literature research, E.R.R., C.T.S., H.S., J.A.C., R.T., S.B.S.; clinical studies, E.R.R., C.T.S., H.S., S.N., R.T., R.H.S., S.B.S.; experimental studies, E.R.R., C.T.S., S.B.S.; statistical analysis, C.T.S., S.B.S.; and manuscript editing, E.R.R., C.T.S., H.S., J.A.C., S.N., S.M.L., R.T., J.P.E., S.B.S.

Funding:
This research was partially supported by the National Institutes of Health (grant 5R21CA131763).

Conflicts of interest are listed at the end of this article.

Table 1

Patient Characteristics

Characteristic	Datum
Total no. of patients	23
No. of men	9 (39)
No. of women	14 (61)
Median age (y)*	60 (42–81)
No. of lesions	29
Median lesion size (cm)*	1.4 (0.6–4.4)
Lesion location	
Liver	21
Lung	6
Adrenal gland	1
Thigh	1
Cancer cell type	
Colon	18 (62)
Lung	3 (10)
Melanoma	2 (7)
Head and neck	2 (7)
Pancreas	1 (3)
Sarcoma	1 (3)
Endometrium	1 (3)
Hepatocellular	1 (3)
Ablation device	
Radiofrequency	17 (59)
Microwave	6 (21)
Irreversible electroporation	5 (17)
Cryoablation	1 (3)

Note.—Unless otherwise indicated, data are the number of patients and data in parentheses are percentages.

* Data in parentheses are the range.

Table 2

Split-Dose FDG PET Parameters

Variable	Datum*
Median uptake time from first FDG injection to preablation PET (min)	78 (40–143)
Median injected first FDG dose (mCi)†	4.2 (3.6–4.4)
Median uptake time for second FDG dose (min)	35 (30–152)
Median injected second FDG dose (mCi)†	8.4 (7.6–8.8)
Average interval between FDG injections (min)	261 (100–450)
Average procedure time from first scan to device removal (min)	166 (84–315)

* Data in parentheses are the range.

† To convert to megabecquerels, multiply by 37.

position with a 15.7-cm cranial-caudal scan range, while the patient's vital signs were continuously monitored. Patients were preoxygenated with a fractional inhaled oxygen concentration of 100% to facilitate artificial suspension of respiration during image acquisition to minimize motion artifacts and allow better registration of PET and CT datasets. Breath-hold planning CT scans of the same region were obtained, and these two datasets were fused to facilitate planning of the optimal electrode trajectory.

Placement of ablation probes was performed in the standard manner for an image-guided ablation by using conventional biopsy mode CT, CT fluoroscopy, or combined US and CT guidance. Breath-hold CT images of the device in position were obtained and were fused with the initial PET dataset to confirm accurate needle position within the FDG-avid target volume. Image guidance for placement of the ablation devices was performed with fused PET/CT fluoroscopy in 26 lesions. Fusion of US with CT/PET imaging was used to target the other three lesions. Fusion of the most recently acquired breath-hold CT images with the PET dataset acquired at the beginning of the procedure was typically repeated multiple times during the procedure. This could be performed easily without the need for repeat PET acquisition, because the patient's position was not changed and the patients were paralyzed. Ablation was then performed as per the manufacturer protocol for the specific ablation device. If necessary, probes were repositioned to create overlapping ablation zones to match the geometry of the lesion and the intended margin.

Once the tumor ablation protocol was complete, the patient was injected with a second dose of approximately 8 mCi (296 MBq) of FDG. Thirty to 45 minutes later, while the patient remained under general anesthesia, repeat breath-hold CT and PET acquisitions were performed at the same table position as the original acquisition for one field of view covering the treated site. Breath-hold contrast-enhanced CT was also performed after the ablation as per the standard protocol at our institution, and this dataset was also fused with the postablation PET dataset.

FDG doses and the time from the dose administration until image acquisition were obtained for all patients. Exponential FDG decay curves were calculated for the median doses. The median uptake time from the first FDG injection to the preablation targeting PET acquisition was 78 minutes (range, 40–143 minutes), and the median injected activity of FDG was 4.2 mCi (155.4 MBq) (range, 3.6–4.4 mCi [133.2–162.8 MBq]). This time varied because the time of the patient's preparation and anesthesia induction also varied. The median uptake time for postablation imaging was 35 minutes (range, 30–152 minutes), and the median injected dose was 8.4 mCi (310 MBq) (range, 7.6–8.8 mCi [281.2–325.6 MBq]). The average interval between FDG injections was 261 minutes (range, 100–450 minutes), and the average procedure time, defined as the time from the first target scan to the removal of the ablation device, was 166 minutes (range, 84–315 minutes) (Table 2). For validation of the imaging findings at the postablation PET, the most recently available follow-up CT, MR, or PET study was used to assess the ablation zone for recurrence.

Statistical Analysis

To estimate the sample size required to evaluate the split-dose method, we used the method described by Eng (15). The prestudy estimate of the recurrence rate was taken to be 5% based on prior interventional (16) and surgery (17) studies. The width of the expected confidence interval was 20%. On the basis of these estimates, we predicted that

this study would require a minimum sample size of 18 ablations.

Results

All lesions were successfully visualized by using the initial reduced approximate 4-mCi (148-MBq) FDG injected activity PET/CT acquisition. No new lesions not previously documented at conventional preprocedure cross-sectional and PET imaging were detected at preablation imaging. A median of three probe positions (range, one to six) were used to achieve the desired ablation size. All ablations were successfully completed according to the preprocedure plan for each patient. In 28 of 29 lesions, no residual PET activity was identified at the immediate postablation PET acquisition. Contrast-enhanced CT performed at the end of ablation also confirmed technical success.

Figure 1 shows the FDG exponential decay curve for the median values of the parameters: an initial FDG dose of 4.2 mCi (155.4 MBq), a preablation uptake time of 78 minutes, a procedure time of 166 minutes, and a postablation dose of 8.4 mCi (310.8 MBq) with an uptake time of 35 minutes. The graph charts the radioactive decay of ^{18}F and demonstrates that the effective FDG activity from which the preablation dataset is acquired is approximately 2.57 mCi (95.09 MBq), whereas the effective FDG activity from which the postablation dataset is acquired is approximately 6.73 mCi (249.01MBq). At the time of the second PET acquisition, the residual activity present from the first injection is approximately 0.65 mCi (24.05 MBq) and therefore contributes minimally to image formation at the second time point. Approximately 90% of the signal for the postablation images comes from the postablation FDG injection and therefore reflects the postablation metabolic state of the tumor.

The only complications noted duringthe ablation procedures were three cases of pneumothorax that required chest tube placement and one pleural effusion treated effi ciently with a short course of prednisone and aggressive bronchodilators. Typical cases are illustrated in Figures 2 and 3. Liver malignancies with significant initial FDG activity were ablated and showed no metabolic activity at postablation FDG PET/CT. This absence of FDG activity was confi rmed at follow-up PET imaging.

In one lesion, FDG uptake was seen at the inferior margin of the lesion after ablation (Fig 4). Biopsy was performed while the patient remained under anesthesia, and immediate on-site cytologic review suggested residual tumor, subsequently confirmed in the final pathologic diagnosis. After replacement of the ablation needle, an additional ablation targeted to the region of persistent FDG activity was immediately performed to ensure complete ablation, and successful ablation of the lesion was confirmed at follow-up imaging (Fig 4c). A retrospective review suggested a lack of complete coverage of the targeted lesion.

The median postablation follow-up imaging for all patients was 155 days (range, 92–257 days). Marginal recurrence was observed in two of 29 (7%) lesions. One recurrence followed ablation of a 4.4-cm lesion close to a major bile duct that was ablated by using irreversible electroporation to reduce the risk of bile duct injury. The second recurrence followed radiofrequency ablation of a caudate lobe lesion adjacent to the main portal vein (Fig 5).

Figure 1

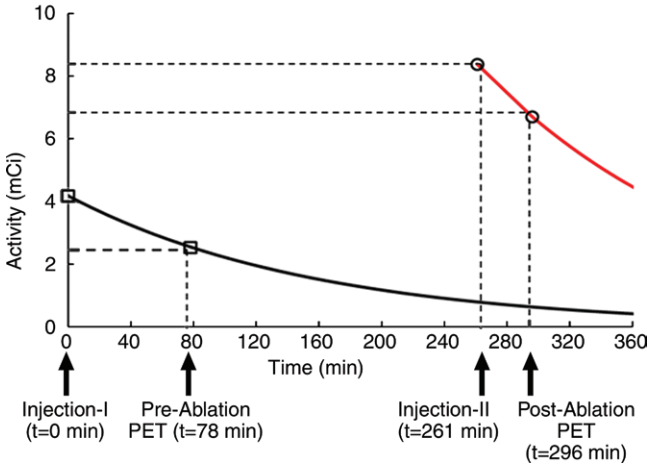

Figure 1: FDG exponential decay curves for the median values of the parameters: an initial injection of 4.2 mCi (155.4 MBq) and a postablation dose of 8.4 mCi (310.8 MBq). Graph charts radioactive decay of the isotope and demonstrates that the effective FDG activity from which the preablation dataset is acquired is approximately 2.57 mCi (95.09 MBq), whereas the postablation activity is approximately 6.73 mCi (249.01 MBq). At second PET acquisition, the residual activity present from the first injection is approximately 0.65 mCi (24.05 MBq) and therefore contributes minimally to the postablation PET images.

Discussion

An important unmet challenge of image-guided ablation has been the lack of clear indicators to the operator that the target lesion has been sufficiently ablated at the conclusion of the procedure. While surgical margins can be evaluated with frozen-section analysis of surgical specimens, this is not practical for ablation. In surgery, if the surgeon has not adequately resected the lesion, the resection can be extended to achieve an appropriate margin. For percutaneous ablation, pathologic evaluation of the margin is currently not feasible. Biopsies of the ablation zone could provide some real-time feedback regarding treatment adequacy.

Figure 3

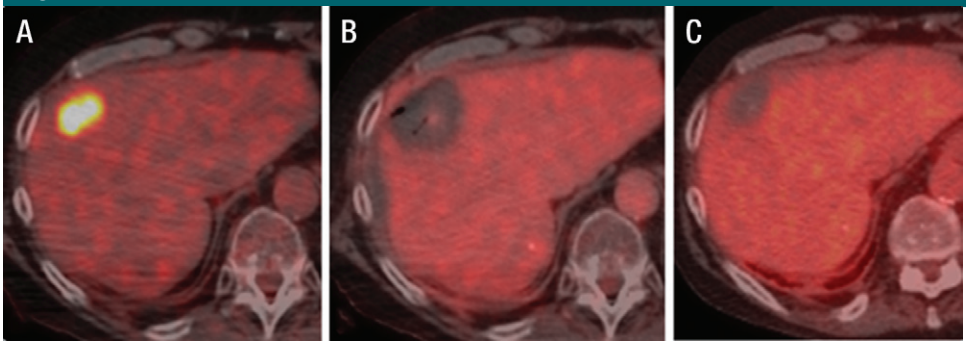

Figure 3: Fused FDG PET/CT images in a 68-year-old man with metastatic colorectal cancer. *A,* Colorectal liver metastasis (standardized uptake value, 9.8). *B,* Intraprocedural image with no metabolic activity and decreased attenuation. *C,* Image of the same ablated area 4 months after the ablation.

Figure 2

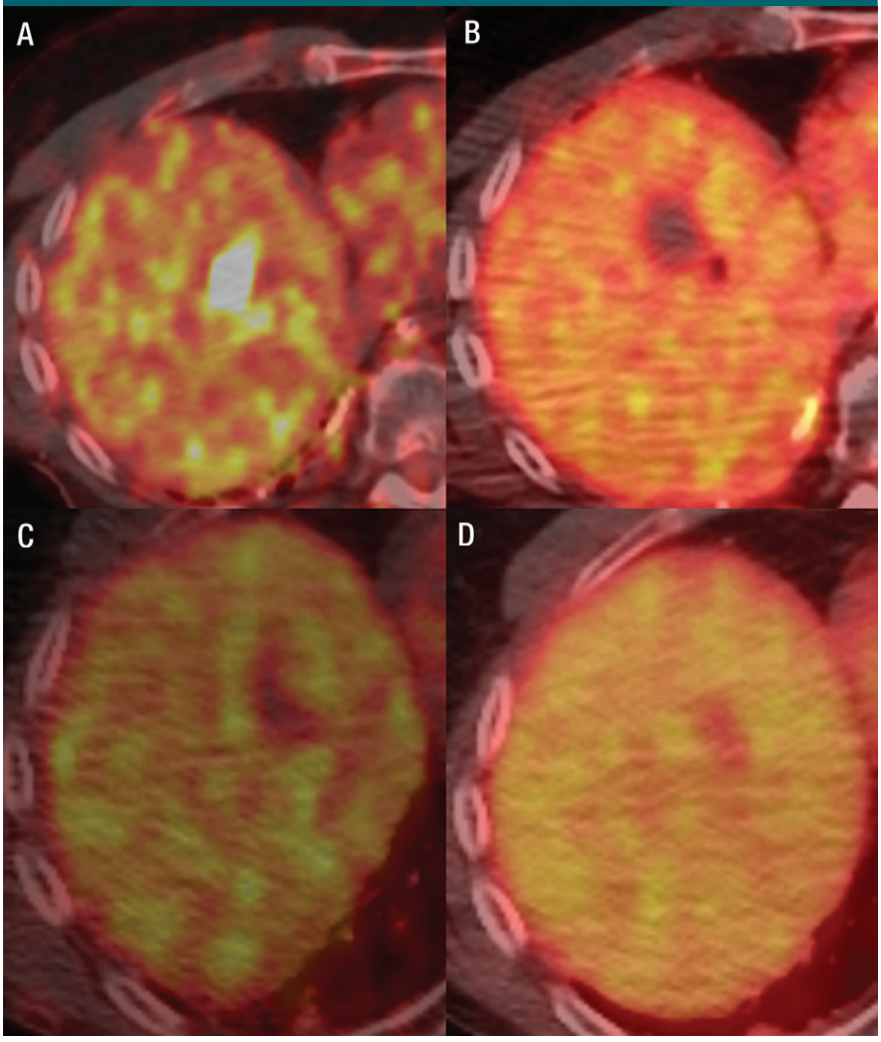

Figure 2: Fused FDG PET/CT images in a 60-year-old man with metastatic melanoma. *A,* FDG-avid liver metastasis in the right lobe (standardized uptake value, 18.2). *B,* Image immediately after microwave ablation shows the photopenic ablation defect. *C,* Image at 4-week follow-up shows good ablation result. *D,* Image 5 months after abaltion shows a further decrease of the ablation zone size and no metabolic activity.

Surrogate indicators used after ablation include measurement of the ablation defect on postablation images and correlation with preprocedure images (18,19), as well as, identification of viable tissue adherent to the radiofrequency probe (20,21).

Use of standard imaging as a surrogate marker of pathologic margin status following ablation is challenging for many reasons. Tissue at the margin of an ablation may not enhance well due to postprocedure edema, injury, or vasoconstriction of the local vasculature but may still retain viable tumor cells. Conversely, normal enhancing tissue can appear as tumor recurrence. Examples of both false-negative and false-positive results are known when CT enhancement characteristics are used to predict ablation adequacy (22–24).

Comparison of postablation imaging with preprocedure imaging may also be difficult due to differences in organ position, patient position, and interval tumor growth between the preprocedure imaging and the procedure date. The use of a two-dose FDG PET/CT as described in our study for both tumor targeting and evaluation of the effectiveness of ablation may be a step toward improving the effectiveness of ablation in the treatment of local primary and metastatic disease. This is different from groups who used a complete FDG dose up front and looked for change immediately after ablation (14) and from other groups who used preprocedure fused PET to guide their ablation procedures (2). Both of these

Figure 4

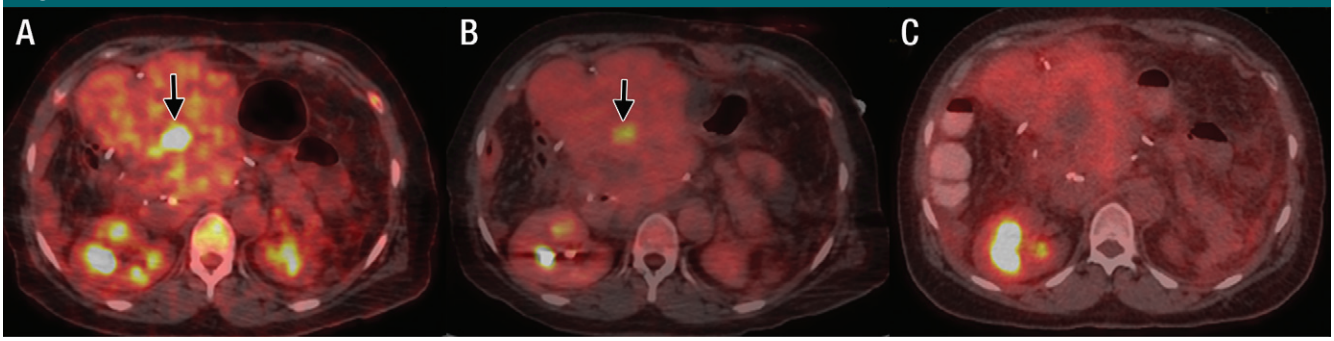

Figure 4: Fused FDG PET/CT images in a 65-year-old woman with metastatic colorectal cancer. *A,* Image prior to ablation shows liver metastasis (arrow), which was treated with radiofrequency ablation (not shown). *B,* Image at the end of ablation shows residual FDG uptake at the inferior margin of the lesion (arrow). *C,* Subsequent follow-up image demonstrates successful repeat ablation.

Figure 5

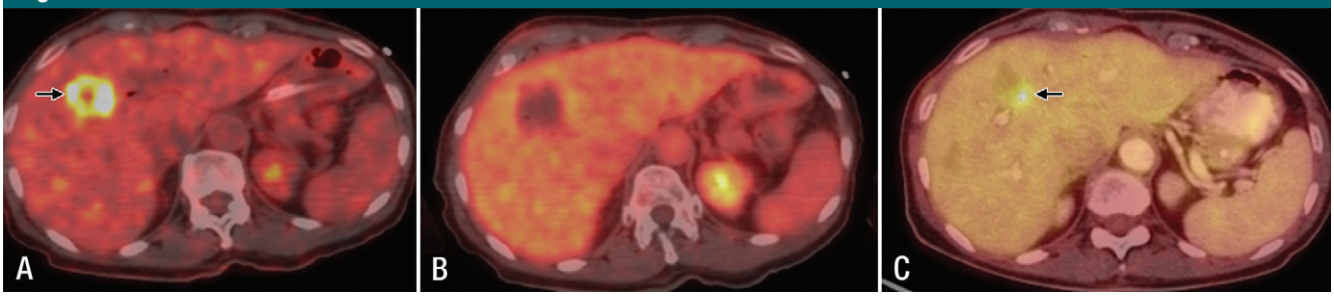

Figure 5: Fused FDG PET/CT images in a 69-year-old woman with metastatic pancreatic cancer. *A,* Image prior to ablation shows liver metastasis (arrow), which was treated with irreversible electroporation (not shown). *B,* Image at the end of ablation shows the ablation zone with no metabolic activity. *C,* Follow-up image at 3 months shows local tumor progression (arrow).

techniques failed to provide evidence of postablation completeness.

We report on a technique of splitting the standard injected FDG dose to enable FDG PET to be used both for guidance during electrode insertion and for endpoint assessment after ablation. This technique relies on the relatively short (110 minutes) half-life of FDG. Most of the activity from the smaller FDG dose used for targeting guidance decays by the time the ablation has concluded. By using our method, the second FDG dose contains about twice the activity as the first. Additionally, a substantial amount of time (mean, 244 minutes) elapses between FDG doses. Consequently, activity from the first (target) dose has largely decayed and activity from the postablation dose dominates during the acquisition of the postablation images. For the patients in our study, the activity from the second FDG dose was approximately 10 times the activity from the original dose by the time the postablation PET scan was acquired.

Cellular uptake of FDG reflects tumor glucose metabolism and is an indicator of viable cells. Absence of FDG uptake suggests absence of viable tumor cells (25). One lesion in our study did show persistent FDG avidity following the postablation FDG injection. We interpreted this finding to indicate the persistence of residual, untreated disease. This was confirmed with biopsy, which triggered immediate additional ablation to this area. Such immediate postprocedure feedback could be compared with intraoperative pathologic evaluation of the surgical margin.

Two lesions that appeared well treated at the postablation PET acquisition developed marginal recurrences during follow-up. Both lesions were in challenging locations: one large lesion, where the technical concern was for injury, was to an adjacent structure (bile duct) and one average-sized lesion was close to a large portal vein branch. We speculate that the postablation PET scans might have been negative in these two cases on the basis of residual viable cancer volume below the threshold for FDG PET detection. One might equate the concept of a R1 resection with microscopic residual disease to an "A1 ablation" with residual disease below the threshold of FDG PET detection (26).

The split-dose protocol used in our study maximizes clinical value for the patient from the radiation exposure associated with FDG activity. Our split-dose protocol (4 mCi [148 MBq] target dose, 8 mCi [296 MBq] treatment efficacy) uses the same total FDG dose as a diagnostic PET (12 mCi [444 MBq]). The 4-mCi (148-MBq) target dose yields sufficient signal to facilitate localization and

targeting of the lesion, even though the images are noisier than typical diagnostic images. However, since all patients had preprocedural diagnostic PET/CT scans, decreased target-to-background ratio was still sufficient to permit localization and guidance. Fusion of the low-dose PET with CT further facilitates accurate lesion identification. This approach is in keeping with the principles of patient radiation dose optimization during other interventional radiologic procedures (27), where greater noise is tolerated for interventional imaging than for diagnostic imaging. When the second injection of FDG is administered, minimal residual activity remains from the initial low activity injection due to the relatively short half-life of the tracer. At the time of postprocedure imaging, the activity from the second injection exceeds residual activity from the first dose by an estimated factor of 10. Therefore, images generated from the second acquisition almost exclusively represent signal from the second FDG injection and portray the metabolic state of the treatment zone. The technique of sequential, differential dosing is well established for other nuclear medicine applications such as cardiac stress testing using technetium 99m-labeled perfusion agents (28).

The use of the split-dose technique also reduces the radiation exposure for the operator and staff during the procedure. We have previously measured radiation exposure to staff from PET-guided procedures using a full 12-mCi (444-MBq) activity dose and found the operator's dose to be in the range of 1–2 mrem (.01–.02 mSv), which is at a very acceptable level considering the annual dose limit of 5000 mrem (5 mSv) (29). With this split-dose technique, the operator and staff are typically in close proximity to the patient for extended periods of time only after the initial 4-mCi (148-MBq) injection. Once the procedure is completed and the second dose of 8-mCi (296-MBq) has been administered, it is uncommon for the operator to be in the room near the patient unless the findings of the postprocedure scan prompt further treatment. Accordingly, this technique should lead to a two-thirds reduction in operator dose compared with standard FDG dosing regimens.

There were several limitations to our study. One potential limitation of this technique might arise from decreased perfusion surrounding the ablation zone due to edema. This can be demonstrated at conventional imaging as an area of reduced enhancement at CT (30). This area of reduced perfusion may contain potentially viable tumor cells, but may not be sufficiently perfused for accurate visualization with standard intravascular contrast agents. We were concerned that this phenomenon might impair delivery of FDG to the region and cause false-negative FDG uptake. There is evidence from neuroimaging, however, that PET tracers are not affected in the same way that conventional blood pool agents are in this regard. In high-grade gliomas treated with antiangiogenic agents such as bevacizumab, contrast-enhanced MR images may show reduced enhancement suggesting tumor response; in contrast, uptake of PET tracers by viable tumor can still be visualized (31). The combination of prolonged uptake time and small molecule size may facilitate the diffusion of FDG through even poorly perfused tissue. A second limitation was the shorter-than-standard uptake time prior to PET imaging after the second FDG dose. The standard uptake time after FDG injection at our institution is approximately 60 minutes for diagnostic PET imaging. In our cases, the uptake time after the second FDG dose was limited to 30–45 minutes. We adopted this shorter uptake time to balance the potential benefits to the patient of obtaining the postablation PET images with the potential risks associated with longer anesthesia times. We also found support for shorter uptake times in prior guidelines from the Society of Nuclear Medicine and other evidence of variable practice in this regard (32,33). In the future, a better understanding of the importance of uptake time for interventional cases needs to be studied. Another limitation of our study was the lack of pathologic confirmation of complete ablation for most patients. Complete ablation was judged on the basis of conventional approaches of image interpretation of follow-up contrast-enhanced images and PET studies correlated with patients' preablation images. Future studies may be needed to pathologically validate the concept.

Finally, the limited availability of PET/CT units for interventional radiology hinders the possibility of a wide spread of the technique. The benefit of being able to avoid a local recurrence with immediate re-treatment needs to be weighed against the extra cost of the technique.

In conclusion, the use of a split-dose technique for FDG PET guidance for percutaneous ablation facilitates targeting of FDG-avid lesions and may provide immediate confirmation of treatment effectiveness. Further studies are warranted to assess the full impact and usefulness of this technique.

Disclosures of Conflicts of Interest: E.R.R. No potential conflicts of interest to disclose. **C.T.S.** No potential conflicts of interest to disclose. **H.S.** No potential conflicts of interest to disclose. **J.A.C.** No potential conflicts of interest to disclose. **S.N.** No potential conflicts of interest to disclose. **S.M.L.** Financial activities related to the present article: none to disclose. Financial activities not related to the present article: author received fees from Imaginab and Molecular Imaging (scientific advisory) for board membership; consultancy fees from Perceptive (imaging CRO); employment from MSKCC Cancer Center; grants P50 CA 84638 (corresponding PI) and R21 CA (renal cell Ca imaging); SKI patents for radiotracers (multiple grant based); travel accommodations with MSKCC compliance); and philanthropic support. Other relationships: none to disclose. **R.T.** No potential conflicts of interest to disclose. **R.H.S.** No potential conflicts of interest to disclose. **J.P.E.** No potential conflicts of interest to disclose. **S.B.S.** Financial activities related to the present article: none to disclose. Financial activities not related to the present article: author received a grant from GE Healthcare. Other relationships: none to disclose.

References

1. Solomon SB, Silverman SG. Imaging in interventional oncology. Radiology 2010;257(3):624–640.
2. Venkatesan AM, Kadoury S, Abi-Jaoudeh N, et al. Real-time FDG PET guidance during biopsies and radiofrequency ablation using multimodality fusion with electromagnetic navigation. Radiology 2011;260(3):848–856.

3. Ayav A, Germain A, Marchal F, et al. Radiofrequency ablation of unresectable liver tumors: factors associated with incomplete ablation or local recurrence. Am J Surg 2010;200(4):435–439.
4. Kim KW, Lee JM, Klotz E, et al. Safety margin assessment after radiofrequency ablation of the liver using registration of preprocedure and postprocedure CT images. AJR Am J Roentgenol 2011;196(5):W565–W572.
5. Kim YS, Lee WJ, Rhim H, Lim HK, Choi D, Lee JY. The minimal ablative margin of radiofrequency ablation of hepatocellular carcinoma (> 2 and < 5 cm) needed to prevent local tumor progression: 3D quantitative assessment using CT image fusion. AJR Am J Roentgenol 2010;195(3):758–765.
6. Kim YS, Rhim H, Cho OK, Koh BH, Kim Y. Intrahepatic recurrence after percutaneous radiofrequency ablation of hepatocellular carcinoma: analysis of the pattern and risk factors. Eur J Radiol 2006;59(3):432–441.
7. Meloni MF, Andreano A, Franza E, Passamonti M, Lazzaroni S. Contrast enhanced ultrasound: should it play a role in immediate evaluation of liver tumors following thermal ablation? Eur J Radiol 2012;81(8):e897–e902.
8. Vilar VS, Goldman SM, Ricci MD, et al. Analysis by MRI of residual tumor after radiofrequency ablation for early stage breast cancer. AJR Am J Roentgenol 2012; 198(3):W285–W291.
9. Deandreis D, Leboulleux S, Dromain C, et al. Role of FDG PET/CT and chest CT in the follow-up of lung lesions treated with radiofrequency ablation. Radiology 2011; 258(1):270–276.
10. Singnurkar A, Solomon SB, Gönen M, Larson SM, Schöder H. 18F-FDG PET/CT for the prediction and detection of local recurrence after radiofrequency ablation of malignant lung lesions. J Nucl Med 2010;51(12):1833–1840.
11. Okuma T, Okamura T, Matsuoka T, et al. Fluorine-18-fluorodeoxyglucose positron emission tomography for assessment of patients with unresectable recurrent or metastatic lung cancers after CT-guided radiofrequency ablation: preliminary results. Ann Nucl Med 2006;20(2):115–121.
12. Liu ZY, Chang ZH, Lu ZM, Guo QY. Early PET/CT after radiofrequency ablation in colorectal cancer liver metastases: is it useful? Chin Med J (Engl) 2010;123(13):1690–1694.
13. Schoellnast H, Larson SM, Nehmeh SA, Carrasquillo JA, Thornton RH, Solomon SB. Radiofrequency ablation of non-small-cell carcinoma of the lung under real-time FDG PET CT guidance. Cardiovasc Intervent Radiol 2011;34(Suppl 2):S182–S185.
14. Sainani NI, Shyn PB, Tatli S, Morrison PR, Tuncali K, Silverman SG. PET/CT-guided radiofrequency and cryoablation: is tumor fluorine-18 fluorodeoxyglucose activity dissipated by thermal ablation? J Vasc Interv Radiol 2011;22(3):354–360.
15. Eng J. Sample size estimation: how many individuals should be studied? Radiology 2003;227(2):309–313.
16. Kuvshinoff BW, Ota DM. Radiofrequency ablation of liver tumors: influence of technique and tumor size. Surgery 2002; 132(4):605–611; discussion 611–612.
17. Curley SA. Radiofrequency ablation of malignant liver tumors. Ann Surg Oncol 2003; 10(4):338–347.
18. Pua BB, Sofocleous CT. Imaging to optimize liver tumor ablation. Imaging Med 2010; 2(4):433–443.
19. Wang X, Sofocleous CT, Erinjeri JP, et al. Margin size is an independent predictor of local tumor progression after ablation of colon cancer liver metastases. Cardiovasc Intervent Radiol 2013;36(1):166–175.
20. Sofocleous CT, Nascimento RG, Petrovic LM, et al. Histopathologic and immunohistochemical features of tissue adherent to multitined electrodes after RF ablation of liver malignancies can help predict local tumor progression: initial results. Radiology 2008; 249(1):364–374.
21. Sofocleous CT, Garg S, Petrovic LM, et al. Ki-67 is a prognostic biomarker of survival after radiofrequency ablation of liver malignancies. Ann Surg Oncol 2012;19(13): 4262–4269.
22. Weight CJ, Kaouk JH, Hegarty NJ, et al. Correlation of radiographic imaging and histopathology following cryoablation and radio frequency ablation for renal tumors. J Urol 2008;179(4):1277–1281; discussion 1281–1283.
23. Lokken RP, Gervais DA, Arellano RS, et al. Inflammatory nodules mimic applicator track seeding after percutaneous ablation of renal tumors. AJR Am J Roentgenol 2007;189(4):845–848.
24. Solomon SB. Can imaging be used to assess treatment success after ablation of renal tumors? Nat Clin Pract Urol 2008;5(12):642–643.
25. Avril NE, Weber WA. Monitoring response to treatment in patients utilizing PET. Radiol Clin North Am 2005;43(1):189–204.
26. Edge SB, Byrd DR, Compton CC, et al, eds. AJCC cancer staging manual 7th ed. New York, NY: Springer-Verlag, 2010.
27. Duncan JR, Balter S, Becker GJ, et al. Optimizing radiation use during fluoroscopic procedures: proceedings from a multidisciplinary consensus panel. J Vasc Interv Radiol 2011;22(4):425–429.
28. Cerqueira MD, Lawrence A. Nuclear cardiology update. Radiol Clin North Am 2001;39(5):931–946, vii–viii.
29. Ryan ER, Thornton RH, Sofocleous CT, et al. PET CT guided interventions: personnel radiation dose. Cardiovasc Intervent Radiol 2012 Nov 15. [Epub ahead of print]
30. Park MH, Rhim H, Kim YS, Choi D, Lim HK, Lee WJ. Spectrum of CT findings after radiofrequency ablation of hepatic tumors. RadioGraphics 2008;28(2):379–390; discussion 390–392.
31. la Fougère C, Suchorska B, Bartenstein P, Kreth FW, Tonn JC. Molecular imaging of gliomas with PET: opportunities and limitations. Neuro-oncol 2011;13(8):806–819.
32. Schelbert HR, Hoh CK, Royal HD, et al. Procedure guideline for tumor imaging using fluorine-18-FDG. Society of Nuclear Medicine. J Nucl Med 1998;39(7):1302–1305.
33. Thie JA, Hubner KF, Smith GT. Optimizing imaging time for improved performance in oncology PET studies. Mol Imaging Biol 2002;4(3):238–244.